Nanoscale Advances

ROYAL SOCIETY OF CHEMISTRY

PAPER

View Article Online
View Journal | View Issue

Cite this: *Nanoscale Adv.*, 2020, **2**, 1228

Effect of the structure and morphology of carbon nanotubes on the vibration damping characteristics of polymer-based composites

Anand Joy, [a] Susy Varughese, [b] Anand K. Kanjarla,[a] Sankaran S.[a] and Prathap Haridoss *[a]

The structure and morphology of the reinforcing material play an important role in the vibration damping characteristics of polymer composites. In this work, multiwalled carbon nanotubes (MWCNTs) with different structures and morphologies are incorporated into a polymer matrix. The vibration damping characteristics of the nanocomposites, in Oberst beam configuration, are studied using a free vibration test in cantilever mode. Inner tube oscillation is established as the vibration damping mechanism by correlating the extent of the loss factor obtained from the two nanocomposites with the dissimilarities in the structure and morphology of the two varieties of MWCNTs. Inner tube oscillation is simulated using molecular dynamics (MD). Since the open-ended double walled CNT (DWCNT) models used in earlier studies over predict the damping, we propose a capped DWCNT model. This can simulate the atomic interactions at the end caps of the tube. This study indicates that the contributions to the observed damping have their origins in the interaction between atoms that constitute the inner and outer tubes rather than the inter-tube frictional energy loss.

Received 31st December 2019
Accepted 2nd February 2020

DOI: 10.1039/c9na00812h

rsc.li/nanoscale-advances

1. Introduction

Polymer based composites combine the viscoelastic properties of the matrix material as well as the interfacial properties of the reinforcing material resulting in enhanced vibration damping.[1] Hence, they are widely used in passive vibration damping applications in aircrafts, automobiles, trains, submarines, ships, *etc.*[1–3] Significant improvement in vibration damping can be achieved by incorporating nano-scale particles as a reinforcement into the polymer matrix.[4,5] The structure and morphology of the reinforcing material affect the damping characteristics of the bulk composite. For example, even though both boron nitride nanotubes (BNNTs) and multiwalled carbon nanotubes (MWCNTs) have a tubular structure, their microstructure is significantly different. The BNNTs have discontinuous "bamboo-like" nodes,[6] whereas the MWCNTs have a continuous tubular structure. Compared to the BNNT reinforced composites, the MWCNT incorporated composites have higher vibration damping.[7] This was attributed to the microstructure of the nano-fillers. The sword-in-sheath or inner tube oscillation mechanism[7] (sliding of the inner tubes) is favoured by the structure of MWCNTs which results in higher energy dissipation.

In another study, CNTs with two or more number of tubes were found to be a better reinforcement for damping application compared to single walled carbon nanotubes (SWCNTs).[8] Molecular dynamics (MD) simulation of lateral oscillation of a SWCNT with chirality (5,5) and a double walled carbon nanotube (DWCNT) which is comprised of an open-ended inner tube and outer tube with chiralities (5,5) and (10,10) respectively was carried out.[9] In the simulation, the individual SWCNT and DWCNT were placed in a cantilever beam configuration and the free end of the cantilever was displaced to set lateral oscillation in them. It is observed that the vibration damping of the DWCNT is an order of magnitude higher than that of the SWCNT. The inner tube oscillation in the DWCNT resulted in higher energy dissipation compared to the SWCNT.

The potential applications of the inner tube oscillation in MWCNTs are in nano-electro-mechanical systems (NEMSs) to build nano-engines, motors, oscillators, *etc.*[10–14] Low friction between adjacent tubes and low wear during inner tube oscillation[11,12] are the other added advantages of MWCNTs for their application in NEMSs.

MWCNTs synthesized by different techniques have significantly different structures and morphologies.[15] The present study focuses on the effect of differences in the structure and morphology of CNTs on the vibration damping behaviour in polymer composites. The MWCNTs considered in this study are synthesized by two well-known methods, *viz.*, plasma arc

[a]*Department Metallurgical and Materials Engineering, Indian Institute of Technology Madras, Chennai 600036, Tamil Nadu, India. E-mail: prathap@iitm.ac.in; Fax: +91 44 2257 0545; Tel: +91 44 2257 4771*

[b]*Department of Chemical Engineering, Indian Institute of Technology Madras, Chennai 600036, Tamil Nadu, India*

discharge and chemical vapor deposition (CVD) techniques. The CNTs synthesized by the plasma arc discharge technique are straight over the entire length (henceforth referred to as straight MWCNTs (sMWCNTs)), whereas those synthesized by CVD are coiled and entangled (henceforth referred to as coiled MWCNTs or cMWCNTs). In this work, we show that the vibration damping characteristics of sMWCNT reinforced epoxy composites are better than those reinforced with cMWCNTs. The micro-structure responsible for the differences in the damping behaviour is simulated using MD. Open ended CNT models used in earlier studies over predict the damping.[16–18] Hence, we propose an end capped CNT model which can simulate the atomic interactions at the tube ends in closed CNTs. The variation of dissipated energy and the dissipation rate with respect to the axial inner wall distance was estimated. The results show the mechanism of damping in CNTs, which originates from the interactions between atoms that constitute the inner and outer tubes.

2. Experimental details

2.1 Materials

The epoxy resin used in this study is based on diglycidyl ether of bisphenol A (DGEBA) and has a viscosity of 450–650 mPa s at 25 °C. The curing agent is polyamidoamine with a viscosity of 10 000–25 000 mPa s at 25 °C. Both were purchased from Huntsman International India Pvt. Ltd. Mumbai, India. Methods adopted in previous research have been followed for the synthesis and purification of arc discharge CNTs.[19] The arc discharge CNTs are referred to as "sMWCNTs". CNTs synthesized by CVD were purchased from Chengdu Organic Chemicals Co., Ltd, China. These CNTs are referred to as "cMWCNTs". This terminology is based on TEM analysis, which is discussed in Section 4.2.

2.2 Fabrication of the epoxy/CNT nanocomposite

Both varieties of CNTs were ultrasonicated in ethanol using a bath ultrasonicator (CREST Ultrasonics, NJ, USA) for 10 min with 25 and 132 kHz frequencies operated in parallel. Epoxy resin was added to the ultrasonicated CNT–ethanol dispersion and stirred for 30 min using a magnetic stirrer. The solution was heated at 85 °C for 10 h to remove ethanol by evaporation. The dispersion was then degassed by keeping it at 40 °C in an oven for 30 min. The curing agent was added to this (ratio of resin to curing agent, 2 : 1 by weight). It was manually stirred using a glass rod for 5 min and then stirred using a magnetic stirrer for 15 min. Finally, it was injected into a Teflon mould lined with silicone rubber. Curing was done for seven days at room temperature. Epoxy composites with 0.5, 1, 2.5 and 5 wt% of CNTs (both cMWCNTs and sMWCNTs) were prepared. Details of the mould and the injection process are described elsewhere.[20,21]

2.3 Material testing and characterization

The free vibration test was conducted according to ASTM E756-05 in Oberst beam configuration (one side damped).[22] 2 mm thick aluminium was chosen as the base material and a 2 mm thick nanocomposite layer was cast on this. The beam dimensions were 200 mm (length) and 10 mm (width). The free length was 180 mm. An initial tip displacement was applied to the beam using an impact hammer (Model 5800B4, Dynapulse, Dytran Instruments). The tip displacement was recorded using an accelerometer (Dytran Instruments) with a sensitivity of 100 mV g^{-1}. The frequency range of the accelerometer was 5 to 10 000 Hz. An NI 9234 data acquisition system from "National Instruments" was used to collect the data through "m+p smart office" application. Loss factors at the first two natural frequencies were calculated by the half power bandwidth method from the frequency response function (FRF). From this the loss factors of the nanocomposites were calculated by using Ross–Kerwin–Ungar (RKU) equations[23] given in the ASTM standard specified above. For a given CNT content, five samples were tested. The average value of the loss factor with standard deviation in the first two modes was plotted against the CNT content.

In order to characterize the nano-scale spacing at the spherical ends of the CNTs, both the varieties were ultrasonicated at 25 kHz and 132 kHz operated in parallel for 10 min in ethanol. A small drop of this was added onto a carbon coated copper grid. It was then examined using an FEI Tecnai T20 TEM operated at 200 kV. For studying the CNT/epoxy interface in the nanocomposite, electron transparent slices were made using a Leica EM UC7 ultramicrotome and examined using an FEI Tecnai T20 TEM. Further high-resolution microscopy analysis was conducted using an FEI Titan TEM operated at 80 kV equipped with an image corrector.

3. Simulation details

The MD simulations were carried out to understand the feasibility of inner-tube oscillations in CNTs contributing to damping and to estimate the energy dissipation. Previous MD simulation studies used open ended CNTs to simulate inner-tube oscillations.[16–18] However, it is observed from the TEM characterization that the CNTs exist with closed ends, like a capped structure. In this study, a CNT model comprising two tubes, a capped (5,5) inner tube and a capped (10,10) outer tube, was used (Fig. 1). The diameter of each tube is determined from the chiral indices (n, m) using the equation $d = \frac{\sqrt{3}a_{C-C}}{\pi}\sqrt{n^2 + m^2 + nm}$, where a_{C-C} = 0.142 nm is the

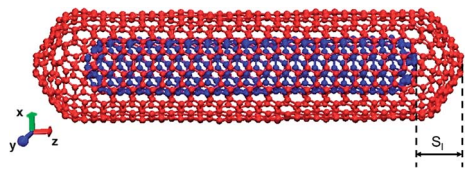

Fig. 1 The model of double walled CNTs (DWCNTs) composed of a (5,5) inner tube and a (10,10) outer tube. The axial inner tube distance (S_i) is marked. The inner and outer tubes have 340 and 880 atoms respectively.

carbon–carbon bond length in the graphene lattice. This set of chiral indices were selected since they result in an inner tube distance, along the radial direction, equal to 3.39 Å. It is close to the realistic value, *i.e.*, 3.4 Å, measured from the TEM images. The spacing between the tubes along the axial direction is termed the axial inner tube distance (S_l). The S_l of the DWCNTs was varied from 2.5 to 10 Å.

The atomic interactions within a tube were described using adaptive inter-molecular reactive bond order (AIREBO) potential.[24] This many-body interaction potential can accurately predict the mechanical properties of CNTs as well as the elastic modulus of graphene.[25–28] The inter tube interactions in DWCNTs were described using Lennard–Jones (LJ) potential. The parameters used for this potential are $\sigma_{C-C} = 3.3407$ Å, $\varepsilon_{C-C} = 0.286$ KJ mol^{-1} and a cut off distance $r_c = 15$ Å.[29] The system energy is minimized by using the conjugate gradient method. This is then equilibrated at 300 K in a canonical ensemble for 0.1 ns. The time step was 0.01 fs. The inner tube was set to oscillation when the outer tube was displaced along the axis towards the inner tube. Oscillations were performed in a micro-canonical ensemble for 0.8 ns with a time step of 1 fs. The LAMMPS software package was used for all the calculations.[30]

4. Results and discussion

4.1 Comparison of the damping behaviour of straight and coiled MWCNTs

The frequency response functions obtained for nanocomposites reinforced with straight and coiled MWCNTs are given in Fig. 2(a) and (b) respectively. Loss factors in mode 1 (η_1) and mode 2 (η_2) are calculated by using the procedure given in Section 2.1 and plotted against the CNT content (Fig. 2(c) and (d)). In both the modes, the nanocomposite with sMWCNTs exhibited the highest loss factor; with the increase of the sMWCNT content, the loss factor increases. In the case of cMWCNT reinforced nanocomposites, the loss factor decreases with the increase of the cMWCNT content. In the first mode, the nanocomposites reinforced with 2.5 wt% sMWCNTs exhibited the highest loss factor. It is around 45% higher than that of neat epoxy. In the second mode, the nanocomposites with 5 wt% sMWCNTs exhibited the highest loss factor. It is around 36.5% higher than that of neat epoxy.

The incorporation of an optimum content of CNTs increased the vibration damping of nanocomposites compared to that of neat epoxy. The trend in the increase is not identical for the two types of nanocomposites. A strong effect of the structure and morphology of CNTs on vibration damping is also observed. The microstructure of these CNTs needs to be analysed to determine the mechanism of vibration damping.

4.2 Microstructure of CNTs

The bright field TEM images of CNTs synthesized by arc discharge and CVD techniques are shown in Fig. 3(a) and (c) respectively. The two varieties of CNTs have distinctly different microstructures. The arc discharge CNTs are straight over the entire length, whereas the CVD CNTs are individually coiled and mutually entangled with many bends and kinks along the length. Selected area electron diffraction (SAED) patterns shown in the inset of Fig. 3(a) and (c) reveal similar reflections for both varieties of CNTs. The pristine nature of their surfaces has been

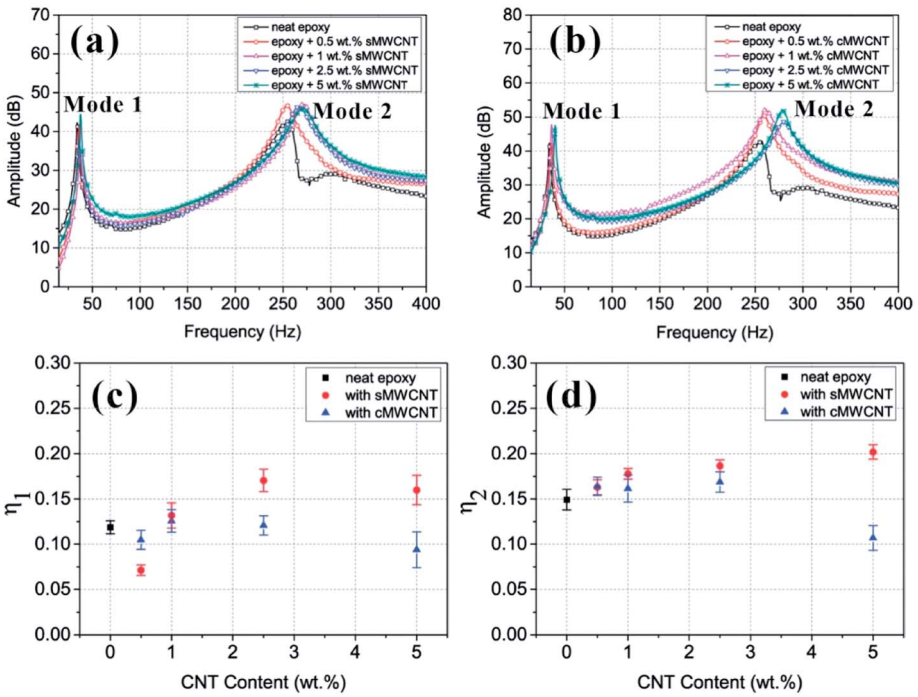

Fig. 2 Frequency response functions of epoxy reinforced with sMWCNTs (a) and cMWCNTs (b). Loss factors in mode 1 (c) and mode 2 (d) are calculated as given in Section 2.1 and plotted against the CNT content.

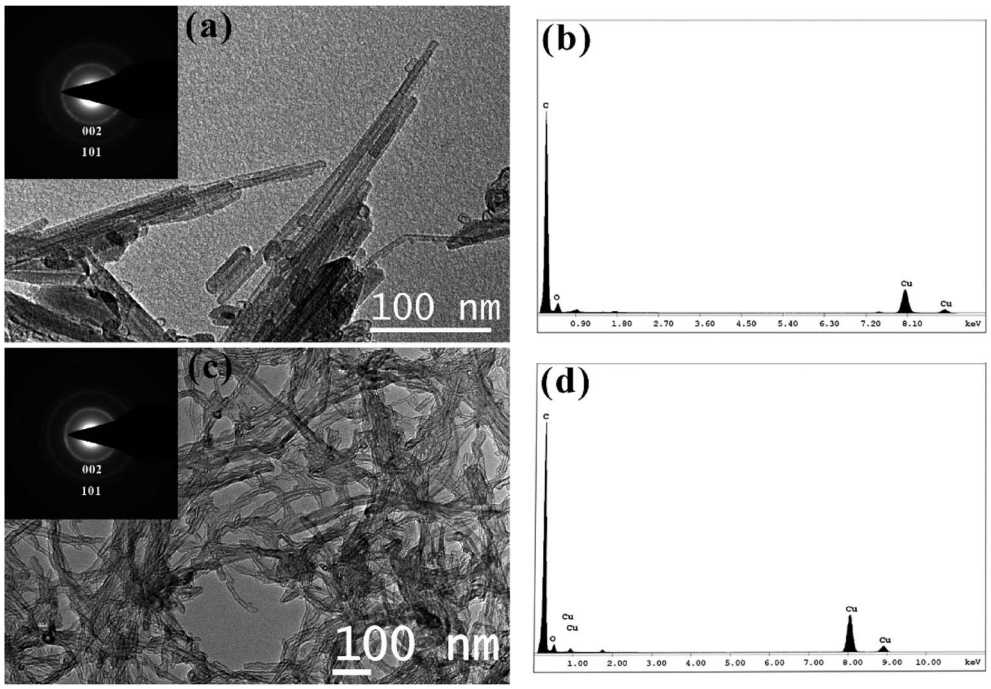

Fig. 3 Bright field TEM images of sMWCNTs (a) and cMWCNTs (c). The corresponding indexed SAED patterns are given as an inset in the respective images. EDS of sMWCNTs and cMWCNTs shown in (b) and (d) respectively reveals the pristine nature of their surfaces.

revealed by the energy dispersive X-ray spectra (EDS) of sMWCNTs and cMWCNTs, which are shown in Fig. 3(b) and (d) respectively. The peaks corresponding to copper are from the supporting copper grids and that corresponding to oxygen could be from copper oxide. The diameter of at least 100 CNTs in both the varieties was measured using ImageJ software from the bright field TEM images. The average diameters of sMWCNTs and cMWCNTs are 15.2 ± 5.5 nm and 16.6 ± 6 nm respectively. The average diameters of both varieties of CNTs are very close, within one standard deviation of each other.

4.3 Molecular dynamics simulation of inner tube oscillation

From the free vibration test, a higher loss factor was obtained for nanocomposites with straight CNTs. The difference in the microstructure between the two types of nanocomposites was characterized by TEM. At a particular CNT content, the only difference between the two types of nanocomposites is in the structure and morphology of CNTs. Inner tube oscillation[17,18,31,32] is favoured by the structure of sMWCNTs. This is due to the uniform cross section over the entire length of this type of CNT (Fig. 4(a)), whereas the kinks and bends in the cross section of coiled CNTs (Fig. 4(b)) hinder the inner tube oscillation. The sMWCNTs are observed to have more number of inner tubes compared to the cMWCNTs, as visible from the TEM images shown in Fig. 4 (inner tubes are marked using white arrows). Also, the input stress in the free vibration test is around 100 times higher than the shear resistant to inner tube oscillation, which is 0.06 MPa (ref. 14) to 0.08 MPa.[13,33]

The inner tube was set to oscillation when the outer tube was displaced towards the inner tube by a few angstroms which depends on the axial inner tube distance, S_I. In the real case, this displacement was assumed to have resulted from the impact force during the free vibration test. At the epoxy–CNT interface, the synergistic effect of van der Waals forces, mechanical interlocking, thermal mismatch and Poisson's contraction results in high interfacial strength.[34] The reported values of interfacial strength are in the range of 70 to 100 MPa.[35,36] Hence, the outer tube is coupled to the epoxy matrix through a continuous interface between the matrix and CNTs. The brightfield TEM images of single CNTs of both sMWCNTs and cMWCNTs dispersed in the epoxy matrix are shown in Fig. 5(a) and (b) respectively. High resolution images show the continuous interlocked epoxy–CNT interface. This indicates that, under the application of an external load, the response of the outer tube is coupled with the epoxy

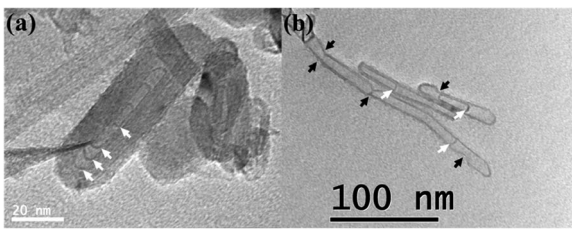

Fig. 4 Bright field high resolution TEM images of sMWCNTs (a) and cMWCNTs (b). Four inner tubes are clearly visible (marked with white arrows) for the sMWCNTs. These tubes are straight over the entire length. The number of inner tubes visible for each of the cMWCNTs is one or two (marked with white arrows in (b)). They are bend and the cross section is not uniform along the length. The kinks and bends of cMWCNTs are marked with black arrows.

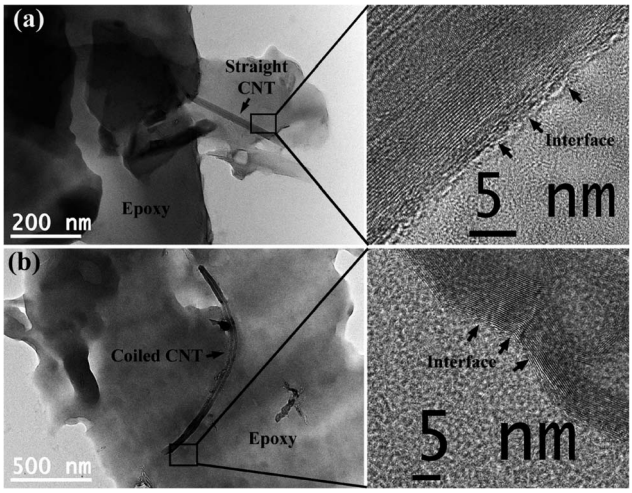

Fig. 5 High resolution bright field TEM images of nanocomposites reinforced with straight MWCNTs (a) and coiled MWCNTs (b) respectively. An individual CNT is spotted in both the cases to observe the interface. A continuous interlocked interface is observed in both nanocomposites.

matrix. However, the inner tubes show a delayed response because of their inertia. This disturbs the stability of the atomic configuration. As a result, the inner tubes oscillate.

One cycle of such oscillation of the inner tube is shown in Fig. 6. The time period of oscillation is observed to be 8 fs. The potential energy of the inner tube for a time interval of 0.8 ns is shown in Fig. 7.

4.3.1 Driving force for the inner tube oscillation. The inner tube oscillation is triggered when the naturally existing

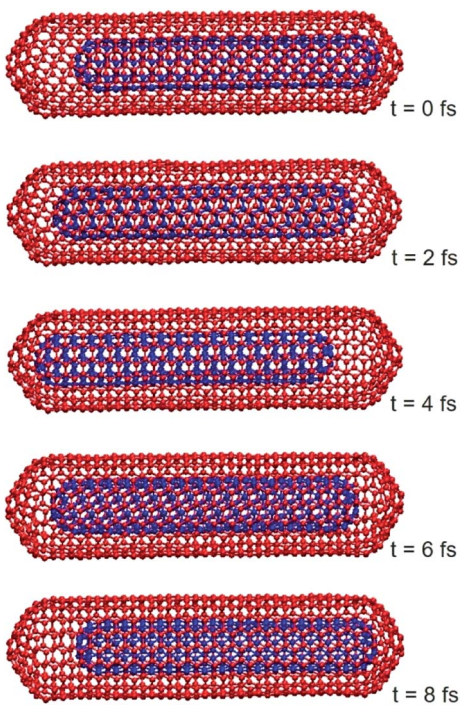

Fig. 6 One cycle of oscillation of the inner tube.

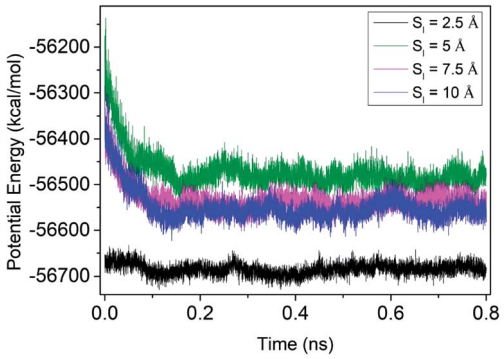

Fig. 7 Variation of the potential energy of the inner tube for various axial inner tube distances, S_l = 2.5, 5, 7.5 and 10 Å.

configuration of MWCNTs is disturbed. The adjacent tubes try to minimize the potential energy, which acts as the driving force for the oscillation. In Fig. 8, the variation of potential energy with time for the DWCNT having S_l = 10 Å is shown. In this case, the oscillation starts at t = 0 ns, which is marked as point A. This is a higher energy state, away from the equilibrium position. This state is achieved by displacing the outer tube towards the inner tube. The position of the carbon atoms at this point is shown in the inset figure A of Fig. 8. The time and potential energy at this point are also given below the respective inset figure.

In this, the atoms in the red colour are of the outer tube and in the blue colour are of the inner tube. The atoms in pale red and pale blue are of the outer and inner tubes but at the diametrically opposite end. The inner tube oscillation starts from point A and stops at point E. Three random points were shown in between the starting and ending of the inner tube oscillation. At point B, the atoms of the inner tube are exactly below the atoms of the outer tube, resulting in higher potential energy. Hence, the oscillation continues to minimize the energy. The potential energy at point C is lower than that at point E. However, the oscillation continued from point C. This is due to the momentum of the inner tubes at point C. It is observed that after 0.363 ns, *i.e.*, at point E, there is no considerable axial displacement for the inner tube. Even though the inner tube oscillation progressed through many lower energy states, the oscillation stops only when the momentum of the inner tube cannot overcome the van der Waals interaction between the tubes. The inner tube tries to minimize the energy further by rotation without a significant axial movement. As a result, a lower energy state, which is marked as point G in Fig. 8, is reached.

4.4 Dissipated energy

The energy dissipated by inner tubes is estimated using

$$\Delta E = E_{\text{Final}} - E_{\text{Initial}} \quad (1)$$

where E_{Final} and E_{Initial} are the potential energies of the inner tube before and after the oscillation. These are the points corresponding to A and E in Fig. 8. Beyond point E, at which

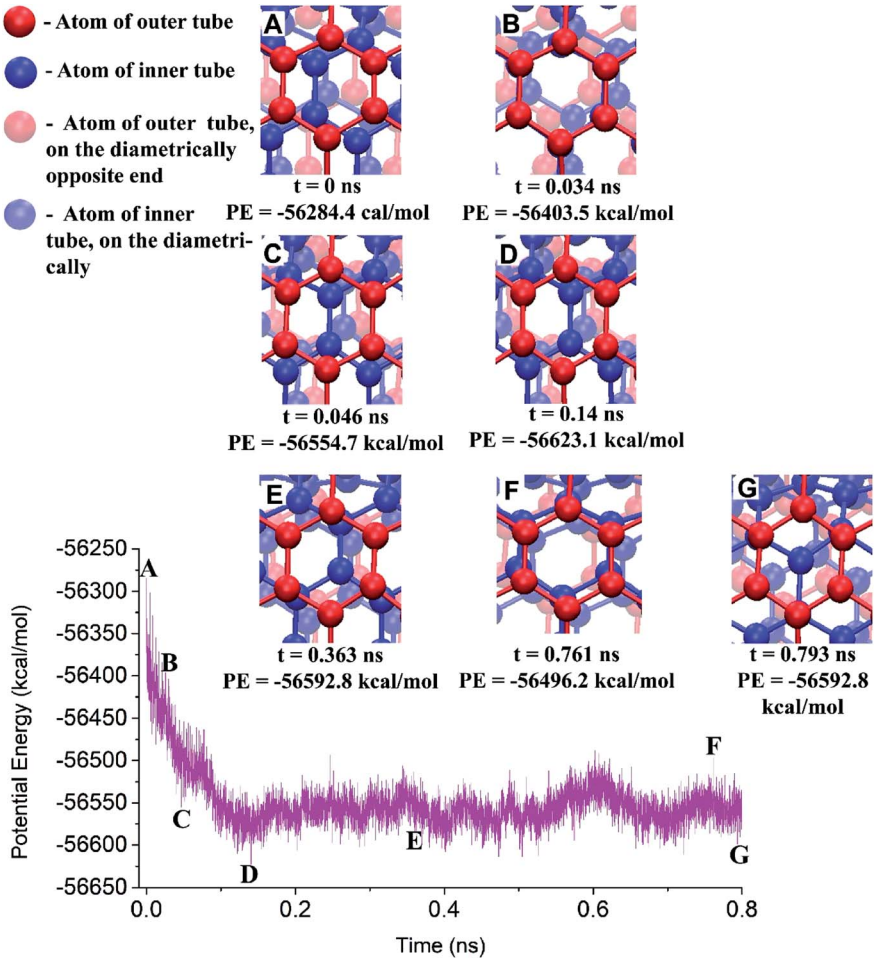

Fig. 8 Variation of potential energy with time during inner tube oscillation of DWCNTs with $S_I = 10$ Å. Corresponding atomic configurations at different times are shown in the inset marked as A to G. The corresponding time and potential energy (PE) are also given. The inner tube oscillation takes place from $t = 0$ ns (point A) to $t = 0.363$ ns (point E).

oscillation stops, the inner tube adjusts its position without any significant axial movement and occupies a lower energy state or local minima, *i.e.*, point G in Fig. 8. The energy dissipated for different S_I is shown in Fig. 9. The energy dissipation rate, *i.e.*, $\dot{E} = \Delta E/\Delta t$, is also shown in Fig. 9. Here, ΔE is given by eqn (1) and Δt is the time taken for inner tube oscillation, which is the time interval between points A and E in Fig. 8. It is found that the energy dissipated and energy dissipation rate increase significantly from $S_I = 2.5$ Å to $S_I = 5$ Å. A small increase is only observed beyond $S_I = 5$ Å. Since the energy dissipated is independent of the sliding distance it may be concluded that the contributions from inter-tube frictional energy loss to the damping is negligible. This study also indicates that the contributions to the observed damping have their origins in the interaction energy between atoms that constitute the inner and outer tubes. The energy dissipation rate decreases slightly for $S_I = 10$ Å from that of $S_I = 7.5$ Å due to the increased oscillation time.

The present study explored interface derived damping, a type of energy dissipation mechanism in which the energy dissipation occurs due to the sliding of available interfaces.[37] In MWCNTs, there are interfaces within each CNT. These tubes act individually and hence are free to slide inside each other.[11] From the loss factor calculated by the free vibration damping test, it is observed that the sMWCNTs are a better reinforcement

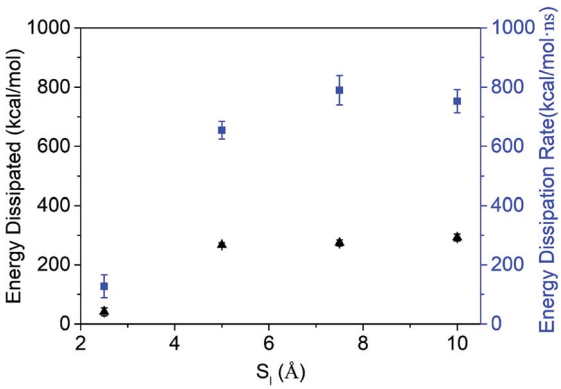

Fig. 9 The variation of energy dissipated and the energy dissipation rate in a DWCNT with different axial inner tube distances, S_I, obtained from MD simulations.

for damping applications than cMWCNTs. From the MD simulation, significant energy dissipation is observed during the inner tube oscillation in a DWCNT. A proportional increase in the dissipated energy can be expected as the number of inner tubes increases.

5. Conclusions

In this work, epoxy resin reinforced with straight and coiled MWCNTs was prepared and subjected to free vibration tests in order to understand the contributions of the microstructure to the vibration damping behaviour. It is observed that the nanocomposites with straight MWCNTs have a higher loss factor compared to those with coiled MWCNTs in the first and second modes. The loss factor increases with increasing concentration of straight CNTs, whereas it levels off with increasing coiled CNT content. The higher damping observed in the case of composites with straight MWCNTs is attributed to the inner tube oscillations. A higher number of inner tubes are observed in the case of straight MWCNTs and inner tube oscillation is favoured in the case of straight MWCNTs due to the uniform cross section over the entire length. However, in the case of coiled MWCNTs, due to the kinks and bends the free sliding oscillations of the inner tubes are hindered. Molecular dynamics (MD) simulations carried out on DWCNTs are used to explain the energy dissipation originating from the inner tube oscillations. The driving force for the oscillation is the minimization of the interaction potential of the inner tubes. The dissipated energy and the rate of dissipation increased significantly when the axial inner tube distance is increased from $S_l =$ 2.5 Å to 5 Å. However, the energy dissipation rate decreased beyond $S_l = 7.5$ Å, resulting from the increased time of inner tube oscillation.

Conflicts of interest

There are no conflicts to declare.

Acknowledgements

The authors gratefully acknowledge the Materials Science Division of the Naval Physical and Oceanographic Laboratory, Cochin, India for the technical discussions and suggestions and the Naval Research Board (NRB) of the Government of India for the financial support.

References

1 R. Chandra, S. Singh and K. Gupta, Damping studies in fiber-reinforced composites–a review, *Compos. Struct.*, 1999, **46**(1), 41–51.
2 M. Kireitseu, D. Hui and G. Tomlinson, Advanced shock-resistant and vibration damping of nanoparticle-reinforced composite material, *Composites, Part B*, 2008, **39**, 128–138.
3 D. D. L. Chung, Review: Materials for vibration damping, *J. Mater. Sci.*, 2001, **36**(24), 5733–5737.
4 S. W. Hudnut and D. Chung, Use of submicron diameter carbon filaments for reinforcement between continuous carbon fiber layers in a polymer-matrix composite, *Carbon*, 1995, **33**(11), 1627–1631.
5 R. Johnson, J. Tang and R. Pitchumani, Characterization of damping in carbon nanotube filled fiberglass reinforced thermosetting-matrix composites, *J. Mater. Sci.*, 2011, **46**(13), 4545–4554.
6 J. Wang, C. H. Lee and Y. K. Yap, Recent advancements in boron nitride nanotubes, *Nanoscale*, 2010, **2**(10), 2028–2034.
7 R. Agrawal, A. Nieto, H. Chen, M. Mora and A. Agarwal, Nanoscale damping characteristics of boron nitride nanotubes and carbon nanotubes reinforced polymer composites, *ACS Appl. Mater. Interfaces*, 2013, **5**(22), 12052–12057.
8 H. Rajoria and N. Jalili, Passive vibration damping enhancement using carbon nanotube-epoxy reinforced composites, *Compos. Sci. Technol.*, 2005, **65**(14), 2079–2093.
9 H. Jiang, M. F. Yu, B. Liu and Y. Huang, Intrinsic energy loss mechanisms in a cantilevered carbon nanotube beam oscillator, *Phys. Rev. Lett.*, 2004, **93**(18), 185501.
10 A. Fennimore, T. Yuzvinsky, W. Q. Han, M. Fuhrer, J. Cumings and A. Zettl, Rotational actuators based on carbon nanotubes, *Nature*, 2003, **424**(6947), 408.
11 J. Cumings and A. Zettl, Low-friction nanoscale linear bearing realized from multi-wall carbon nanotubes, *Science*, 2000, **289**(5479), 602–604.
12 A. N. Kolmogorov and V. H. Crespi, Smoothest bearings: interlayer sliding in multiwalled carbon nanotubes, *Phys. Rev. Lett.*, 2000, **85**(22), 4727.
13 Q. Zheng and Q. Jiang, Multiwalled carbon nanotubes as gigahertz oscillators, *Phys. Rev. Lett.*, 2002, **88**(4), 045503.
14 J. L. Rivera, C. McCabe and P. T. Cummings, Oscillatory behaviour of double-walled nanotubes under extension: a simple nanoscale damped spring, *Nano Lett.*, 2003, **3**(8), 1001–1005.
15 J. Sumfleth, K. Prehn, M. H. Wichmann, S. Wedekind and K. Schulte, A comparative study of the electrical and mechanical properties of epoxy nanocomposites reinforced by cvd-and arc-grown multi-wall carbon nanotubes, *Compos. Sci. Technol.*, 2010, **70**(1), 173–180.
16 M. V. Prasad and B. Bhattacharya, Molecular dynamics simulations of carbon nanotube based oscillators having topological defects, *Int. J. Nanosci.*, 2011, **10**(01n02), 355–359.
17 P. Tangney, S. G. Louie and M. L. Cohen, Dynamic sliding friction between concentric carbon nanotubes, *Phys. Rev. Lett.*, 2004, **93**(6), 065503.
18 W. Guo, Y. Guo, H. Gao, Q. Zheng and W. Zhong, Energy dissipation in giga-hertz oscillators from multiwalled carbon nanotubes, *Phys. Rev. Lett.*, 2003, **91**(12), 125501.
19 A. J. Berkmans, S. Ramakrishnan, G. Jain and P. Haridoss, Aligning carbon nanotubes, synthesized using the arc discharge technique, during and after synthesis, *Carbon*, 2013, **55**, 185–195.
20 A. Joy, S. Varughese, S. Shanmugam and P. Haridoss, Multiwalled carbon nanotube reinforced epoxy

nanocomposites for vibration damping, *ACS Appl. Nano Mater.*, 2019, **2**, 736–743.

21 A. Joy, S. Varughese, S. Shanmugam and P. Haridoss, Role of interface on damping characteristics of multi-walled carbon nanotube reinforced epoxy nanocomposites, *Mater. Res. Express*, 2019, 1050c4.

22 E756-05(2010) A, in *Standard test method for measuring vibration-damping properties of materials*, ASTM International, West Conshohocken, PA, 2010.

23 D. Ross, E. Ungar and E. Kerwin, *Structural damping*, ASME, 1959, pp. 49–88.

24 S. J. Stuart, A. B. Tutein and J. A. Harrison, A reactive potential for hydrocarbons with intermolecular interactions, *J. Chem. Phys.*, 2000, **112**(14), 6472–6486.

25 H. Zhao, K. Min and N. R. Aluru, Size and chirality dependent elastic properties of graphene nanoribbons under uniaxial tension, *Nano Lett.*, 2009, **9**(8), 3012–3015.

26 K. Dilrukshi, M. Dewapriya and U. Puswewala, Size dependency and potential field influence on deriving mechanical properties of carbon nanotubes using molecular dynamics, *Theor. Appl. Mech. Lett.*, 2015, **5**(4), 167–172.

27 V. R. Coluci, S. O. Dantas, A. Jorio and D. S. Galvão, Mechanical properties of carbon nanotube networks by molecular mechanics and impact molecular dynamics calculations, *Phys. Rev. B: Condens. Matter Mater. Phys.*, 2007, **75**, 075417.

28 J. Zhao, N. Wei, Z. Fan, J. W. Jiang and T. Rabczuk, The mechanical properties of three types of carbon allotropes, *Nanotechnology*, 2013, **24**(9), 095702.

29 A. Kutana and K. Giapis, Transient deformation regime in bending of single-walled carbon nanotubes, *Phys. Rev. Lett.*, 2006, **97**(24), 245501.

30 S. Plimpton, Fast parallel algorithms for short-range molecular dynamics, *J. Comput. Phys.*, 1995, **117**(1), 1–19.

31 S. Legoas, V. Coluci, S. Braga, P. Coura, S. Dantas and D. S. Galvao, Molecular-dynamics simulations of carbon nanotubes as gigahertz oscillators, *Phys. Rev. Lett.*, 2003, **90**(5), 055504.

32 X. Zhang, G. Santoro, U. Tartaglino and E. Tosatti, Dynamical phenomena in fast sliding nanotube models, *Philos. Mag.*, 2013, **93**(8), 922–948.

33 M. F. Yu, B. I. Yakobson and R. S. Ruoff, Controlled sliding and pullout of nested shells in individual multiwalled carbon nanotubes, *J. Phys. Chem. B*, 2000, **104**(37), 8764–8767.

34 K. K. Ang and K. S. Ahmed, An improved shear-lag model for carbon nanotube reinforced polymer composites, *Composites, Part B*, 2013, **50**, 7–14.

35 X. Chen, L. Zhang, M. Zheng, C. Park, X. Wang and C. Ke, Quantitative nanomechanical characterization of the van der waals interfaces between carbon nanotubes and epoxy, *Carbon*, 2015, **82**, 214–228.

36 C. A. Cooper, S. R. Cohen, A. H. Barber and H. D. Wagner, Detachment of nanotubes from a polymer matrix, *Appl. Phys. Lett.*, 2002, **81**(20), 3873–3875.

37 D. Chung, Interface-derived solid-state viscoelasticity exhibited by nanostructured and microstructured materials containing carbons or ceramics, *Carbon*, 2018, 567–581.